J. Phys. Res. Edu., Vol. 2, March 2025

Study of the mechanical properties of CdS_2 and its enhanced optoelectronic performance under Mn doping: a first principles study

Bhawana Thapa and Amit Shankar*

Condensed Matter Theory Research Lab, Department of Physics, Kurseong College, Darjeeling 734203, India

Using density functional theory, a first-principles calculation was conducted to investigate the optoelectronic and mechanical properties of CdS_2. The material exhibits semiconductor behavior with an indirect band gap of 1.3 eV under the GGA approach, which increases to 2.4 eV with mBJ correction. The pristine sample displays ductile characteristics and ionic bonding among its constituent atoms. Substituting Mn at the Cd site reduces the energy band gap while enhancing the material's optical response. The pure CdS_2 demonstrates favorable optical properties, including significant optical absorption, which is further improved by Mn doping. These features make CdS_2 a promising candidate for optoelectronic applications such as photovoltaic devices, light emitters, and detectors.

I. INTRODUCTION

With the rising demand for energy, the world is increasingly turning to renewable resources and advanced materials to meet the needs of a technologically evolving society. While many optoelectronic devices are commercially available, scientists and engineers continue to innovate, especially in areas like solar cells and renewable energy. Despite dominating 95% of the market, the brittleness and low optical absorption coefficient of Silicon make it unsuitable for thin-film and flexible solar cells [1–3], particularly in high power-to-weight applications [4]. The development of optoelectronic devices began with the invention of LEDs and semiconductor lasers in the 1960s. The devices in question use the photovoltaic effect, an important interaction between light and matter, to emit or detect electromagnetic radiation in the visible and near-infrared frequency. Examples include LEDs, laser diodes, photodetectors, optical amplifiers, and modulators, which manipulate photons much like electrons in a circuit. Semiconducting materials are key to these devices, and Group III nitrides stand out for their direct band gap, cost-efficiency, and ability to create robust, efficient devices, making them ideal for laser diodes, LEDs, and photodetectors [5].

The foundation of optoelectronic devices lies in the electronic band gap and optical properties, such as absorption coefficient and dielectric constant of the material. In this context transition metal dichalcogenides (TMDCs) have gained much attention for their diverse physical, electrical, and optical characteristics. With a sizable bandgap in the visible to near-infrared (NIR) range (1–2 eV), TMDCs are ideal for optoelectronic sensors and light-emitting sources in short-range optical communication [6]. These compounds have the

chemical form MX_2, where X is a chalcogen (S, Se, or Te) and M is a transition metal. With a 1–2 eV energy gap and high absorption coefficients (105 cm^{-1}), TMDCs are ideal for solar energy absorption, making them a promising alternative to traditional solar cells [7, 8]. The tuning of physical properties of TMDCs are essential for extending their functionality and can be achieved through substitution or chemical doping [9]. The previous studies show that doping with elements like Mn, Ni, and Re enhances optical [10] and magnetic [13] properties. For instance, Ni-doped $\mathrm{MoS_2}$ improves photocatalytic activity and visible absorbance [12] , while V and Mn doping in $1\mathrm{T}-\mathrm{ZrSe_2}$ effectively modulates the electronic and magnetic properties for spin injection [13]. Cadmium dichalcogenides ($\mathrm{CdX_2, X = S, Se, Te}$) are part of the TMDC family and hold significant potential for industrial and optoelectronic applications. These materials crystallize in a pyrite-type cubic structure and exhibit semiconducting behavior with a notably flat conduction band [14]. $\mathrm{CdTe_2}$ and $\mathrm{CdSe_2}$, in particular, demonstrate high absorption coefficients [15] and optical properties suitable for photovoltaic applications. Additionally, Jia et al. [16] reported remarkable thermoelectric performance for $\mathrm{CdSe_2}$ and $\mathrm{CdS_2}$, with figures of merit reaching 2.29 and 1.37 for p-type doping, and 1.16 and 0.57 for n-type doping, respectively. This makes their mechanical, electronic, and optical properties highly intriguing for both theoretical and experimental exploration.

Due to their well-known electrical and optical features, cadmium dichalcogenides are outstanding choices for optoelectronic applications. However, among this family,$\mathrm{CdS_2}$ remains underexplored despite its potential for advancing modern technologies. Our study was motivated by the absence of thorough research to investigate the electrical, mechanical, and optical characteristics of $\mathrm{CdS_2}$ in order to fully realize its promise for photovoltaic and optoelectronic applications. In the meantime, density functional theory (DFT) has shown itself to be an effective computational technique for making very accurate predictions about the physical characteristics of solids.In this study, we perform an exhaustive examination of $\mathrm{CdS_2}$ using the full-potential linearized augmented plane-wave (FP-LAPW) method within the DFT framework. In order to comprehend its optoelectronic properties, we investigate its electronic structure, mechanical behavior, and optical response functions, which involve complex dielectric constants and optical absorption. Additionally, we also investigate low concentration Mn doping at Cd site, to improve its optical response which aims to make $\mathrm{CdS_2}$ a potential for next-generation technological applications.

II. SIMULATIONS

Electronic properties were calculated from first principles using DFT and the FP-LAPW method, which was implemented in the Wien2k code [17] which is widely regarded as one of the most efficient methods for simulating ground-state properties of materials [18, 19]. The Perdew-Burke-Ernzerhof (PBE) parameteriza-

tion of the generalized gradient approximation (GGA) [20] was utilized for the exchange-correlation energy of electrons. The $\mathrm{R_{MT}} \times \mathrm{K_{max}} = 8$, which establishes the matrix size necessary to attain convergence of the energy eigenvalues, was used in the computations. In this expression, K_{max} is the maximum modulus for the reciprocal lattice vectors, and $\mathrm{R_{MT}}$ is the smallest muffin-tin radius. For all calculations, the $\mathrm{R_{MT}}$ for Cd, Mn, and S were set to 2.8, 2.2, and 1.8 $\mathrm{a.u.}$, respectively. The self-consistent potential computations were performed using a dense k-mesh of $15 \times 15 \times 15$, with a self-consistency convergence level of 10^{-4} Ry. Up to $\mathrm{G_{max}} = 13\ \mathrm{a.u.}^{-1}$, the interstitial region's charge density was expanded as a Fourier series with wave vectors. The first-principles calculations within GGA as exchange-correlation functional typically underestimate the band gap, failing to accurately predict the gap. This was addressed by determining the electrical characteristics using the modified Becke-Johnson (mBJ) exchange potential [21, 22]. For simulating doped structures such as $\mathrm{Cd_{1-x}Mn_xS_2}$, we used a $2 \times 2 \times 2$ supercell, which consists of 32 Cd and 64 S atoms. For a doping concentration of x = 0.75, 24 Cd atoms are replaced by Mn, which can occur in many different configurations. Among these, configurations involving corner atoms were chosen due to their symmetric environment and nearly identical energy levels. Nonetheless, the Mn atom combinations that were most energetically advantageous were chosen. Other concentrations were treated in the same way.

III. STRUCTURAL, ELASTIC PROPERTIES AND STABILITY

The pyrite-type $\mathrm{CdS_2}$ crystallizes in a cubic structure (space group $\mathrm{Pa\bar{3}}$) as illustrated in Fig. 1. The Wyckoff positions of Cd and S in this structure are 4a (0, 0, 0) and 8c (0, 0, u), respectively. The internal parameter u, which dictates the position of the sulphur atom, depends entirely on the system's chemical composition. In this study, the optimized value of u is 0.406, aligning well with previously reported values [15]. The space group's symmetry requirements dictate the locations of the other atoms inside the unit cell. Through structural optimization, which involved modifying the unit cell parameters to reduce the material's total energy, the crystal structure attributes of $\mathrm{CdS_2}$ were determined. This process stabilized the structure in its energetically favourable form. The optimized lattice constant was determined to be 6.425 $\mathring{A}$, which is consistent with earlier findings [15]. The formation energy (ΔE_F) of the sample, calculated as -0.16 Ry using Eq. (1) [23], confirms the thermodynamic stability of the system

$$\Delta E_F = \frac{E_{Tot} - aE_{Cd} + bE_S}{a+b}, \tag{1}$$

where E_{Tot} is the total energy of the system, a and b represent the number of Cd and S atoms with their equilibrium energy E_{Cd} and E_S, respectively.

The unmarred sample's mechanical characteristics were examined. Using the Voigt-Reuss-Hill (VRH)

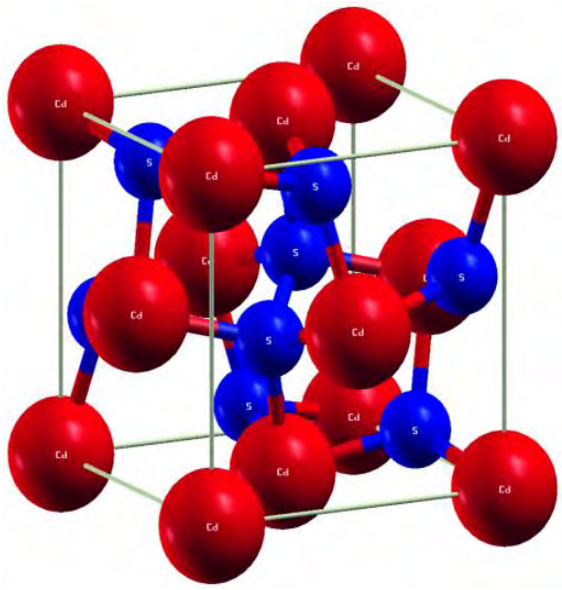

FIG. 1. Crystal structure of CdS_2.

approximation, other elastic parameters, including the bulk modulus (B), Young's modulus (Y), and shear modulus (G), were calculated using the independent elastic constants (C_{11}, C_{12}, and C_{44}) for the cubic structure, which were obtained using volume conservation techniques [24]. The detailed relationships between the independent elastic constants and the derived elastic parameters can be found in reference [25]. The estimated elastic parameters at ambient conditions, derived after accounting for volume deformation, are presented in Table. I. The mechanical stability requirements are met by these values [26], specifically $C_{11} + 2C_{12} > 0, C_{44} > 0, C_{11} - C_{12} > 0$. The data in Table. I indicate that the sample is more resistant to compression along the X-axis and exhibits weaker resistance to pure shear deformation, as reflected by $C_{11} > C_{12}$. A comparison with the literature reveals that the bulk modulus of the sample is higher than those of its family members containing Se and Te [27, 28], indicating its superior resistance to compressibility. The shear modulus (G) and Young's modulus (Y) represent the stiffness of the material against elastic deformation under external forces. Among cadmium dichalcogenides, the shear modulus follows the order $CdSe_2 > CdS_2 > CdTe_2$ [27, 28], with a similar trend observed for Y. Furthermore, the Pugh's ratio and Poisson's ratio (ν) indicate the ductile nature of the material with ionic bonding [29].

IV. OPTOELECTRONIC PROPERTIES

The electronic properties describe the behavior and state of electrons within a material, which can be analyzed by examining the energy band structure. The link between the momentum and energy of carriers in a

Alloy	C_{11}	C_{12}	C_{44}	B	Y	G	B/G	ν
CdS_2	87.57	52.43	47.62	64.04	51.23	19.32	2.5	0.36
Prev.[30]	95.62	50.04	29.47	65.23	70.07	26.52	2.4	0.32

TABLE I. Calculated elastic constants C_{11}, C_{12}, C_{44}, bulk modulus (B), Young's modulus (Y), isotropic shear modulus (G) in GPa, Pugh's ratio B/G and Poisson's ratio (ν) for CdS_2.

solid is represented by this structure. The density of states (DOS) indicates the number of states available at each energy level for occupation. To determine if a material is semiconducting, metallic, or insulating based on the scale of the energy gap between the highest occupied and lowest unoccupied states, it is essential to analyze the DOS and band structure[30–32]. Since optical spectra are directly related to the energy band structure and can be characterized by the dielectric function $\varepsilon(\omega)$, they offer a potent way to examine a material's electrical properties and possible optoelectronic applications. Because of their remarkable qualities, such as their significant absorption in the solar spectrum, transition metal dichalcogenides (TMDCs) have been thoroughly investigated for their photovoltaic [34] and photocatalytic [33] applications. With an indirect band gap of 1.3 eV, CdS_2's semiconducting nature is revealed by the energy band structure and DOS plots (Fig. 2). This result aligns with previous GGA-based theoretical findings [15]. Incorporating mBJ into

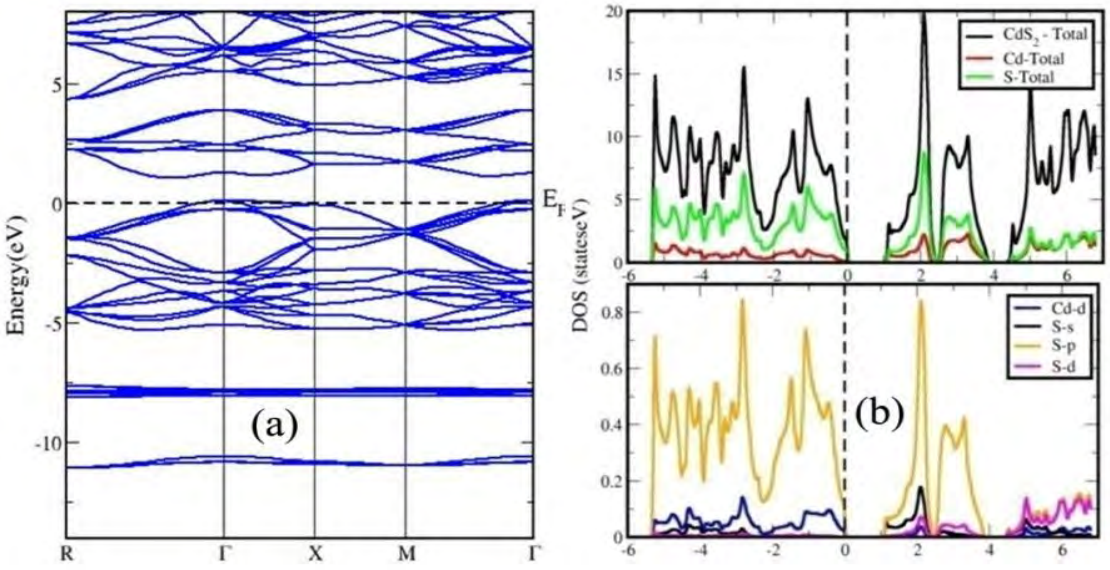

FIG. 2. (a) Energy band structure and (b) density of states of CdS_2.

the calculations increases the band gap to 2.4 eV, which is in qualitative consensus with the experimental report in reference [14]. The DOS analysis shows that the Cd-d bands are located below the S-p bands,

indicating significant hybridization between the metal and chalcogen states.

In order to increase the capacity and functionality of TMDCs, a dopant is necessary for altering the host lattice's band structure. One efficient method for this is to use substitutional doping to tune the electrical characteristics of TMDCs [9]. The consequence of doping on the electrical characteristics of CdS_2 across various dopant concentrations is examined in this section. The DOS and band structure results for specific compositions showing notable variations are presented in Fig. 3. When Mn atoms substitute Cd sites, the electronic band gap reduces to 0.99 eV and 1.06 eV for 50% and 75% doping, respectively. The drop is explained by the conduction bands' (CBs') downward shift, which creates an indirect band gap. Even with complete substitution of Cd atoms by Mn, the material retains its semiconducting nature with a band gap of 1.02 eV. Furthermore, Mn doping significantly enhances the material's optical properties.

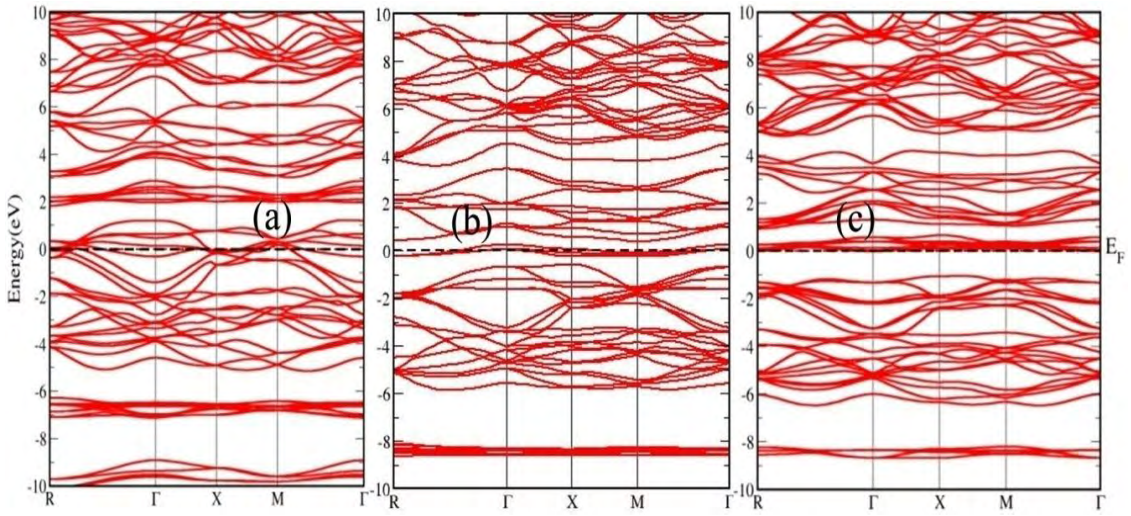

FIG. 3. Energy band structure of $Cd_{1-x}Mn_xS_2$ (a) x = 0.25, (b) x = 0.50 and (c) x = 0.75 by GGA.

To evaluate the material's response to incident photons, a critical factor for photovoltaic activity, the optical absorption and dielectric constants were analyzed, as shown in Fig. 4. The addition of Mn atoms at the Cd site significantly alters the optical characteristics, with MnS_2 exhibiting the highest static dielectric constant, $\varepsilon_1(0)$ of 229.15 among the pure dichalcogenides. The real part of the dielectric function $\varepsilon_1(\omega)$ changes from a positive to a negative value as photon energy grows. A boost in the density of free charge carriers is linked to this phenomenon, suggesting that the incident photons are reflected off the surface of the material. Beyond 3.0 eV, $\varepsilon_1(\omega)$ stabilizes, suggesting transparency at high-energy radiations, which is advantageous for applications such as lens manufacturing. Mn doping also enhances the absorption coefficient in the high-energy range, achieving a maximum value of 123.86×10^4 cm^{-1} for MnS_2 at 4.5 eV. All of the materials under investigation show potential as wide-spectrum photovoltaic materials due to their

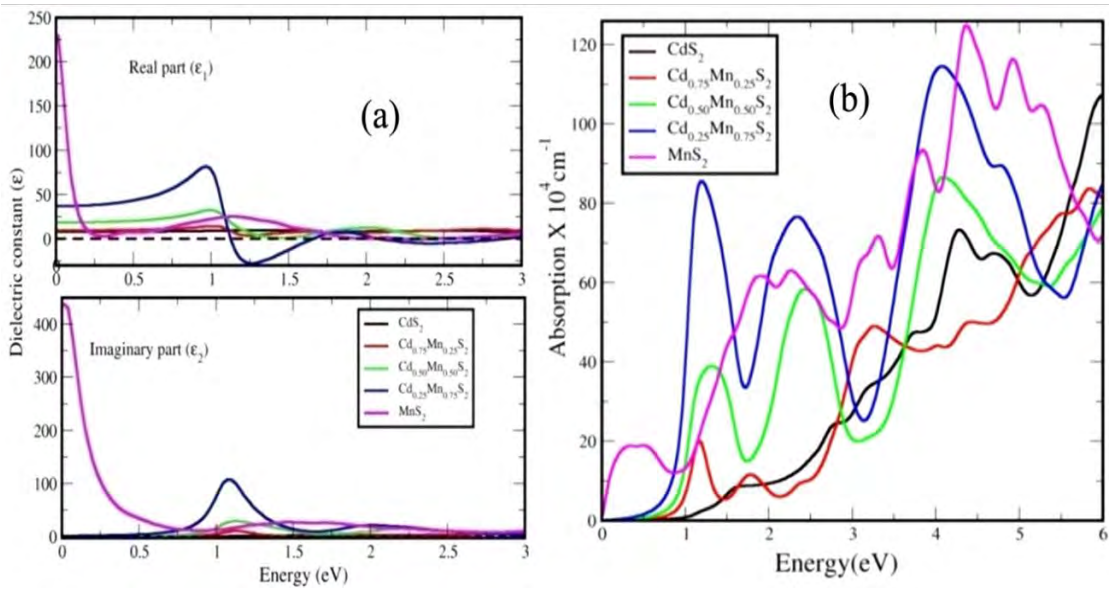

FIG. 4. (a) Dielectric function, (b) absorption coefficient of $Cd_{1-x}Mn_xS_2$.

capacity to absorb light in the visible, ultraviolet, and near-infrared wavelengths. The optical and electronic properties of the alloys vary with dopant concentration and photon energy, expanding their potential for diverse applications in optoelectronic fields, such as thin-film growth and advanced optoelectronic devices.

V. CONCLUSIONS

The mechanical, electrical, and optical properties of CdS_2 are systematically investigated in this research, emphasizing the possibility for optoelectronic applications. The material exhibits a ductile nature with ionic bonding between its constituent atoms and demonstrates a high resistance to deformation. CdS_2 is a semiconductor with an indirect band gap of 1.3 eV, which increases to 2.4 eV when calculated using the mBJ potential. It also shows a favorable optical response, including significant optical absorption. The effect of Mn doping is particularly notable, as it slightly reduces the band gap while enhancing the material's optical properties, such as the dielectric constant and overall optical response. Because of this enhancement, Mn-doped CdS_2 is better suited for a variety of optical applications. Additionally, the study suggests that doping at the transition metal site offers a promising avenue for further enhancing the absorption coefficient, depending on the specific alloy under investigation.

ACKNOWLEDGMENTS

A. S. acknowledges DST-SERB, India for research funding (EEQ/2017/000319).

* amitshan2009@gmail.com

[1] S. Philipps, Photovoltaics Report, Fraunhofer Institute for Solar Energy Systems (2020).

[2] S. Jeong, D. Michael, Mc Gehee and Yi Cui, Nat. Commun. **4**, 2950 (2013).

[3] M. O. Reese *et al*, Nat. Energy **3**, 1002 (2018).

[4] L. Qingfeng *et al*, Nano Energy **22**, 539 (2016).

[5] M. Razeghi, IEEE Photonics J. **3**, 263 (2011).

[6] Y. F. Chen *et al*, Nanotechnology **27**, 445705 (2016).

[7] S. Khalid *et al*, J. Mater. Chem. C **3**, 46 (2015).

[8] M. S. Fuhrer and J. Hone, Nat. Nanotechnol. **8**, 146 (2013).

[9] N. Onofrio, D. Guzman and A. Strachan, J. Appl. Phys. **122**, 185102 (2017).

[10] L. J. Kong, G. H. Liu and L. Qiang, Comput. Mater. Sci. **111**, 416 (2016).

[11] P. Zhao, J. Zheng, P. Guo, Z. Jiang, L. Cao and Y. Wan, Comput. Mater. Sci. **128**, 287 (2017).

[12] G. Yongji *et al*, Nano Lett. **14**, 442 (2014).

[13] X. Zhao, T. Wang, C. Xia, X. Dai, S. Wei and L. Yang, J. Alloys Compd. **698**, 611 (2017).

[14] T. A. Bither, R. J. Bouchard, W. H. Cloud, P. C. Donohue and W. J. Siemoks, Inorg. Chem. **7**, 2208 (1968).

[15] P. Olsson, J. Vidal and D. Lincot, J. Phys.: Condens. Matter **23**, 405 (2011).

[16] T. Jia, C. Jesús, K. H. Madsen, Z. Yongsheng and W. Su-Huai, Phys. Rev. B **105**, 245203 (2022).

[17] P. Blaha, K. Schwarz, G. K. H. Madsen, D. Kvasnicka and J. Luitz, Comput. Phys. Commun. **59**, 399 (1990).

[18] K. M. Wong, S. M. Alay-e-Abbas, Y. Fang, A. Shaukat and Y. Lei, J. Appl. Phys. **114**, 034901 (2013).

[19] Y. Zhu, Y. C. Cheng and U. Schwingenschlögl, Phys. Rev. B **84**, 153402 (2011).

[20] P. Perdew, K. Burke and Y. Wang, Phys. Rev. B **54**, 16533 (1996).

[21] A. D. Becke and E. R. Johnson, J. Chem. Phys. **124**, 221101 (2006).

[22] W. Feng, D. Xiao, Y. Zhang and Y. Yao, Phys. Rev. B **82**, 235121 (2010).

[23] A. Yakoubi, O. Baraka and B. Bouhafs, Results Phys. **2**, 19 (2012).

[24] W. Voigt, Adv. Earth Sci. **1**, 1 (1928); A. Reuss and Z. Angew, J. Appl. Math. Mech. **9**, 49 (1929); R. Hill, Proc. Phys. Soc. Sect. A **65**, 349 (1952).

[25] I. Benkaddour *et al*, Mater. Sci. Semicond. Process. **185**, 108974 (2025).

[26] M. Born and K. Huang, Oxford: Clarendon (1954).

[27] A. A. Musari, D. P. Joubert and G. A. Adebayo, Physica B: Condens. Matter **552**, 159 (2019).

[28] T. Chatterji *et al*, Phys. Rev. B **91**, 1104412 (2015).

[29] F. Pugh, Philos. Mag. **45**, 823 (1954).

[30] C. Stampfl, W. Mannstadt, R. Asahi and A. J. Freeman, Phys. Rev. B **63**, 155106 (2001).

[31] I. N. Remediakis and E. Kaxiras, Phys. Rev. B **59**, 5536 (1999).

[32] Y. I. Matsushita, K. Nakamura and A. Oshiyama, Phys. Rev. B **84**, 075205 (2011).

[33] W. K. Ho, J. C. Yu, J. Lin, J. G. Yu and P. S. Li, Langmuir **20**, 5865 (2004).

[34] E. Gourmelon *et al*, Sol. Energy Mater. Sol. Cells **46**, 115 (1997).